Supercontinuum generation in a microstructured optical fiber by picosecond self Q-switched mode-locked Nd:$GdVO_4$ laser

2007 Laser Phys. Lett. 4 413

(http://iopscience.iop.org/1612-202X/4/6/001)

Abstract: An effective supercontinuum (SC) generation is demonstrated by injecting picosecond self Q-switched mode-locked Nd:$GdVO_4$ laser pulses into a 1-m long microstructured fiber. The laser is operated at wavelength 100-nm away from the longer zero-dispersion of this dual zero-dispersion wavelength microstructured fiber. The phenomena of modulation instability, stimulated Raman effect, and dispersive wave can be sequentially observed from experimental results, leading to spectral broadening as pumping increases.

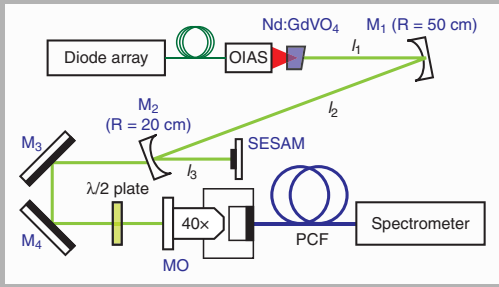

Schematic diagram of experimental setup of SC generation

Supercontinuum generation in a microstructured optical fiber by picosecond self Q-switched mode-locked Nd:$GdVO_4$ laser

J.-H. Lin, [1] *K.-H. Lin,* [2] *C.-C. Hsu,* [3] *W.H. Yang,* [3] *and W.-F. Hsieh* [3,*]

[1] Department of Electro-optical Engineering and Institute of Electro-optical Engineering, National Taipei University of Technology, Taipei 10608, Taiwan
[2] Department of Science, Taipei Municipal University of Education, 1, Ai-Kuo West Rd., Taipei 100, Taiwan
[3] Department of Photonics and Institute of Photonics, National Chiao Tung University, 1001, Tahsueh Rd., Hsinchu 300, Taiwan

Received: 27 December 2006, Revised: 12 January 2007, Accepted: 14 January 2007
Published online: 24 January 2007

Key words: nonlinear optics; nonlinear fiber optics; supercontinuum; microstructured fiber; Q-switched mode locking

PACS: 42.65.-k, 42.65.Dr, 42.60.Gd, 42.55.Xi

1. Introduction

Supercontinuum (SC) generation from nonlinear microstructured fibers (MFs) has been widely used in optical coherent tomography, optical metrology, coherent spectroscopy, and nonlinear microscopy, etc. The remarkable performance of MFs are due to their unique properties of tailorable dispersion and high nonlinear coefficient by modifying the fiber structure [1]. The desired dispersion and nonlinearity properties of guided modes in MFs can be produced by specially designed array of air holes in the fiber cladding or core [2–4]. Generally, high peak power is the key factor for spectral broadening to result in SC generation in MFs. Therefore, femtosecond continuous wave mode-locked (CW-ML) lasers, including Ti:Sapphire laser and Cr:Forsterite laser, etc., are often used as the pumping sources to generate SC, that only several mini-watts of average power can easily make the peak power reach a few kilowatts .

When the femtosecond laser is launched into the nonlinear MFs, various nonlinear optical effects including self-phase modulation (SPM), modulation instability (MI), higher-order soliton breakup, self-frequency shift by stimulated Raman scattering (SRS), and four-wave mixing (FWM), etc., will be induced to cause spectral broadening [5–9] or optical frequency conversion [3,4,10–13]. The anti-Stokes emission from MFs can be efficiently generated by modifying the air holes and controlling the bire-

* Corresponding author: e-mail: wfhsieh@mail.nctu.edu.tw

fringent [3, 4, 10]. Besides, the Cherenkov emission is ideally suited for selective coupling into the high order guided modes in MFs that are both experimentally and numerically demonstrated [11]. Through the mode control, the switching between the regime of broadband emission generation and the regime of isolated spectral components are experimentally observed [12]. In addition, a nonlinear transformation of pulses into higher order mode of a specifically designed few-mode MFs will produce high-quality spectrally isolated hollow beams [13].

The peak power is relatively low in CW-ML picosecond lasers due to their longer pulsewidths and therefore high average powers are required for SC generations. For example, CW-ML laser with 10 ps pulsewidth and 2.4 W of average power was used to generate SC from 700 nm to 1600 nm while the launching wavelength is located in the anomalous dispersion region of fiber [14]. For higher peak power, additional technique such as cavity-dumping was needed to produce sub-kilowatt picosecond pulses for generating more than 600 nm bandwidth of SC in MFs, and the fiber length is longer than 3 m [15, 16]. Sub-nanosecond Q-switched laser pulses with sub-kilowatt peak power have also been used to generate SC by launching them into endless single mode MFs [17]. In addition, ultra-wide and flat SC could be generated by using dual-wavelength pumping at 1064 nm and 532 nm [18].

Recently, Nd:$GdVO_4$ has become of great interest in Nd-doped laser crystals due to their wider bandwidth and better thermal properties in comparison with Nd:YVO_4 and Nd:YAG. Various mode-locking techniques, including semiconductor saturable absorber mirror (SESAM) [19] and nonlinear mirror (NLM) [20], have been used for ultrashort pulse generation. Before entering the completely CW-ML state, a Q-switched ML (QML) state can be observed in Nd:$GdVO_4$ laser systems as the pump power increases [19–21]. Distinguished from Q-switched pulses, the CW-ML pulses are contained in the Q-switching envelope to retain the characteristics of ultrashort laser pulses, but the pulse repetition rate is reduced. Therefore, higher peak power can be achieved at lower average power for QML pulses without using the cavity dumping technique.

In a previous work we have studied the build-up of supercontinuum in heated MF using a CW-ML femtosecond Ti:Sapphire laser [9]. As compared with the MF at room temperature, a new blue-shifted spectral component is observed in the initial stage of SC generation. Besides, NLM mode-locking of a diode-pumped Nd:$GdVO_4$ laser in use of a 10 mm long KTP crystal [20] was demonstrated by us to generate stable CW-ML at relative low threshold pump power of 2.3W. In this paper, we use picosecond QML pulses from a diode-pumped Nd:$GdVO_4$ laser by SESAM to generate SC effectively from an 1-m-long MF with dual zero-dispersion wavelengths.

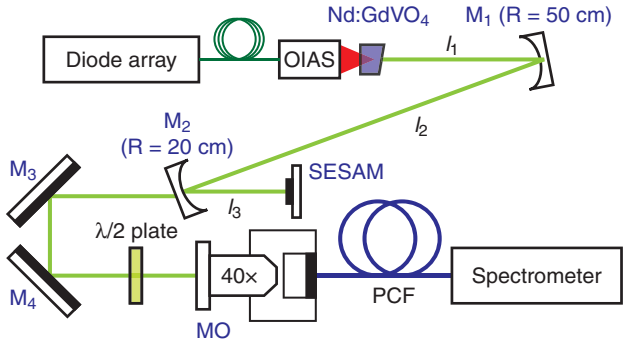

Figure 1 (online color at www.lphys.org) Schematic diagram of experimental setup of SC generation. M_1 and M_2 are folding mirrors of the oscillator. M_3 and M_4 are two flat mirrors used for collimating of light. MO is $40\times$ microscope objective lens used for focusing light into the PCF

2. Experimental setup

Fig. 1 shows the experimental setup of SC generation using our homemade Nd:$GdVO_4$ laser as the injection source. Laser pulses from the oscillator are collimated by two reflective mirrors and then focused into a 1-m-long polarization maintaining MF (Crystal Fibre, PM 760) by a $40\times$ microscope objective lens. A $\lambda/2$ plate is used to change the polarization of the laser pulses before they are injected into the MF. Finally, we measured the output spectrum from MF by an optical spectrum analyzer (Ando, AQ-6315). By optimizing the injected light field into the MF and properly rotating the $\lambda/2$ plate, we can obtain the widest broadened output spectrum from the MF with about 35% coupling efficiency.

The schematic figure-z laser setup (Fig. 1) consists of a $4 \times 4 \times 8$ mm a-cut Nd:$GdVO_4$ crystal that is end-pumped by the fiber coupled diode arrays (Coherent Inc., FAP-81-16C-800-I) of 808 nm in wavelength. The pump beam coming out from the fiber is imaged on the crystal through the $1 : 1.8$ optical imaging accessories (OIA's, Coherent Inc.). One side of the laser crystal is high-reflection (HR) coated at 1064 nm and anti-reflection (AR) coated at 808 nm. The other side of the crystal with 2° wedge is AR coated at 1064 nm. The laser cavity consists of two concave mirrors: one mirror M_1 (the radius of curvature $R = 500$ mm) is HR coated at 1064 nm. The other mirror M_2 ($R = 200$ mm) having reflectivity of 80% at 1064 nm is used as the output coupler. The flat SESAM (modulation depth 1.6%, absorbance 3%, damage threshold 600 MW/cm^2, Batop Inc.) is placed at the end of the cavity. The lengths l_1 (from laser crystal to the M_1), l_2 (M_1 to M_2), and l_3 (M_2 to SESAM) are 30 cm, 80 cm, and 11 cm, respectively.

At pump power P_p of 6 W, we maximized output powers of Nd:$GdVO_4$ to obtain regularly stable CW-ML pulse trains. Then, we measured the output power versus the pump power shown in Fig. 2 without touching the laser

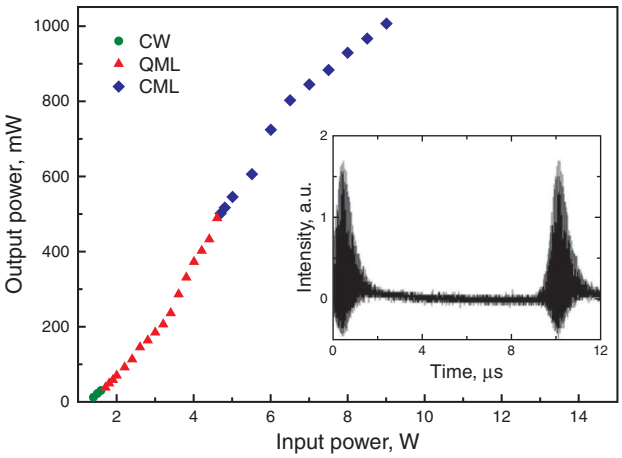

Figure 2 (online color at www.lphys.org) Output powers of Nd:$GdVO_4$ versus the input pump power at different states of CW (green circles), QML (red triangles), and CW-ML (blue diamonds). Inset is the time trace of QML pulses

β_2, ps^2/km	β_3, ps^3/km	β_4, ps^4/km	$\beta_5 \times 10^6$, ps^5/km	$\beta_6 \times 10^8$, ps^6/km
−34.64518	−0.01037	0.00132	−11.6922	9.10398

Table 1 Parameters of dispersion at 1064 nm

cavity. As the pump power is increased, we found the output power increases, accompanied by the changing of laser state from CW (green circles), QML (red triangles), to CW-ML. While the pump power is tuned between the 1.7 W and 4.6 W, we always observe QML pulse train, however, the Q-switching envelope experiences small variation and timing jitter. Therefore, we needed to properly adjust the length of l_3 and the SESAM to optimize loss modulation depth. Then, the stable time traces of QML pulses will be displayed on the oscilloscope (inset of Fig. 2) that reveals constant shape of Q-switching envelope with successive equal time spacing (the repetition rate is about 120 kHz). Each Q-switching envelope has the width of about 1 μs (FWHM), in which about one hundred CW-ML pulses are contained. The time spacing between the CW-ML pulses is 8 ns, which corresponds to the cavity round trip time. The pulsewidth of QML pulses is about 15 ps (FWHM), and the center wavelength is 1062.9 nm, corresponding to the anomalous dispersion region of the MF.

Fig. 3a shows the scanning electron microscope (SEM) image of the cross section of the used polarization maintaining MF. This fiber has high birefringence resulting from the difference in the diameters of the three air-hole pairs closest to the core: one pair of air holes has larger diameter (0.7 μm) and the other two pairs smaller (0.6 μm). The core diameter is about 1.7 μm and the pitch Λ (spacing between adjacent holes) is about 1.4 μm. The fiber has two zero dispersion wavelengths at 760 nm and 1160 nm,

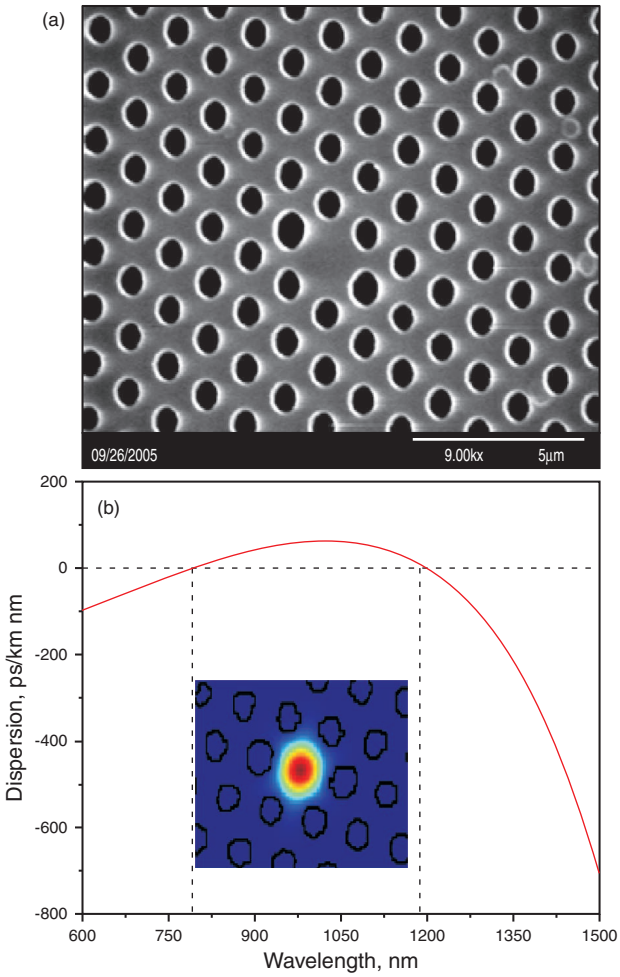

Figure 3 (online color at www.lphys.org) (a) The SEM for the cross section of the MF (scale bar 5 μm), and (b) calculated dispersion curves and mode pattern by the "mode solutions" using the image of (a)

respectively (from the product specification). Using the SEM image as the input to the software Mode Solutions (Lumerical Solutions Inc.), we can calculate the dispersion curve as well as the mode pattern for this MF, and the result are shown in Fig. 3b. Our calculation result shows that the two zero-dispersion wavelengths are located at 790 nm and 1190 nm, which is slightly different from the product specification. This may be due to the distortion from the shadows around the air holes in SEM image. In addition, the coefficient β_n listed in Table 1 represents the n_{th} order Taylor expansion of the propagation constant around the carrier frequency ω_0, which are obtained from the calculated dispersion of Fig. 3b.

3. Results and discussion

Due to the lower repetition rate of QML envelope than CW-ML pulses, the peak power of QML pulses are about

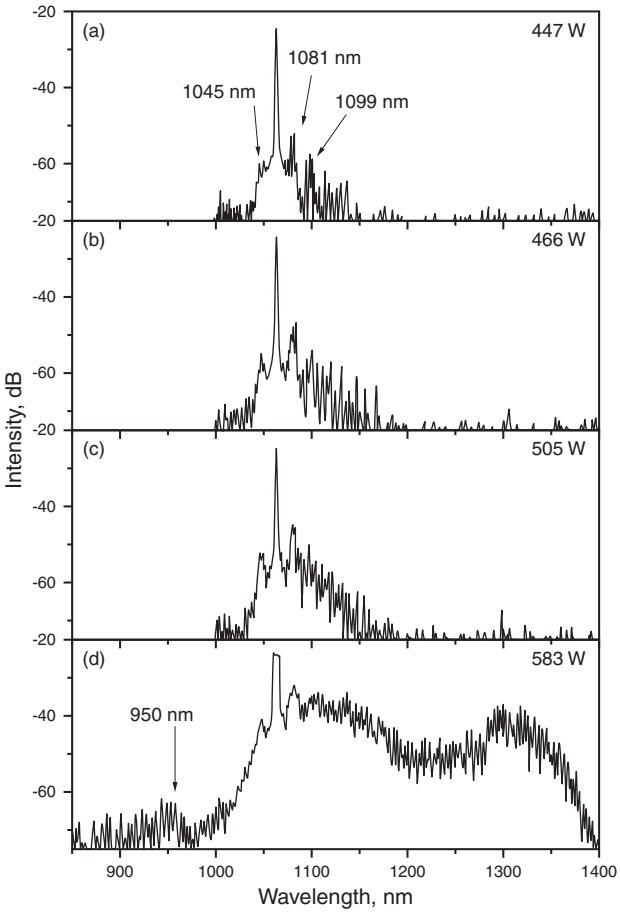

Figure 4 The evolutions of spectral broadening for the experimental observation at the peak power of (a) 447 W, (b) 466 W, (c) 505 W, and (d) 583 W, respectively

20 times higher than CW-ML pulses. Therefore, several nonlinear effects, such as MI and SRS effects, can be induced in MFs even at lower average powers. We injected QML pulses into the MF to observe the spectral broadening phenomena. Fig. 4a–Fig. 4d show the evolution of spectral broadening as the average power of injected laser pulses are increased from 230 mW to 300 mW, which correspond to the peak power of 447 W to 583 W. Here, we estimate the peak power of QML pulses injected into the MFs by considering the coupling efficiency of 35%, pulsewidth of 15 ps, envelope repetition rate of 120 kHz, and about one hundred pulses in each Q-switching envelope.

For injected peak power of 447 W, spectral peaks appear at 1045 nm, 1081 nm, and 1099 nm, respectively, on the broadened spectrum curve of Fig. 4a. These spectral peaks are resulted from MI, while the pump wavelength is located at the anomalous dispersion region of the fiber. Due to interplay between the nonlinear and dispersive effect, Stokes and anti-Stokes components are generated from the amplitude and phase perturbations. The frequency shifts of these components relative to the center wavelength of the pumping are $\nu_n = \pm\Omega_n/2\pi$, and the maxima of new frequency components are

$$\Omega_n = n\left(\frac{2\gamma P_0}{|\beta_2|}\right)^{\frac{1}{2}}, n = 1, 2, \ldots, \quad (1)$$

where $\gamma = (n_2\omega_0/cA_{eff})$ is the nonlinear coefficient with n_2 being the nonlinear refractive index and A_{eff} being the effective core area. Due to relative small core diameter, very large value of $\gamma \simeq 74$ km^{-1}W^{-1} around 1064 nm exists in our MF. In Fig. 4a, the frequency shifts of the first two harmonics ν_1 and ν_2 (with ν_1 corresponding to 1045 nm, 1081 nm, and ν_2 corresponding to 1099 nm) relative to the pumping (1062.9 nm) are 4.8 THz and 9.2 THz, which can be described by Eq. 1. Due to the Raman gain, the amplitude of 1045 nm peak is smaller than that of 1081 nm and only the Stokes component of the second harmonic at 1099 nm can be observed, but not the anti-Stokes component. When the gain exceeds the threshold power of Raman amplification, the Stokes components within the Raman band are amplified. The amplified Stokes components can be regarded as the pump to induce second or even higher order Stokes components, and the red edge of the spectrum is shifted to longer wavelength, i.e. self-frequency shift. The red-shift of spectrum suppresses the gain of anti-Stokes components and results in stronger amplitude of Stokes component on the red side of the pump than the anti-Stoke component on the blue side. As the average injected power is increased further, the Raman-effect becomes more obvious and makes the spectrum edge move toward even longer wavelengths (see Fig. 4b and Fig. 4c).

There is a rapid evolution in spectral broadening from Fig. 4c to Fig. 4d when the peak power is increased from 505 W to 580 W. Fig. 4d shows that the spectrum spans from 900 nm to 1400 nm for average pumping power of 300 mW (or peak power of 580 W). Once the spectrum extends to exceed the longer zero-dispersion wavelength, an additional spectral component would be generated at 1315 nm (Fig. 4d). It is termed dispersive wave and is resulted from the perturbation of the higher order dispersive parameter β_n ($n \geq 3$) near the zero-dispersion wavelength. The higher order dispersion offers phase-matching to make the energy of the pump be transferred to the dispersive wave. Besides, there is an additional peak at 950 nm that might be due to the degenerate four-wave mixing (DFWM) of the pump pulses and the dispersive wave.

4. Conclusion

Picosecond self Q-switched mode-locked pulses can be produced at lower pump power from Nd:$GdVO_4$ laser in use of semiconductor saturable absorber mirror. Due to lower repetition rate and higher peak power of Q-switched mode-locked pulses than CW mode-locked pulses at the

same average power, the QML pulses can be used to effectively generate supercontinuum in microstructured fiber as short as only 1 m. Supercontinuum spectra from 900 nm to 1400 nm were experimentally demonstrated although the pumping wavelength is 100 nm away from the longer zero-dispersion wavelength. Nonlinear effects, such as modulation instability, stimulated Raman effect, and higher-order dispersion perturbation at the zero-dispersion wavelength sequentially predominates the SC generation as the pumping power increases.

Acknowledgements This work is partially supported by the National Science Council of Taiwan, Republic of China, under grant NSC-95-2221-E-009-308, NSC-95-2745-M-009-002, and NSC 95-2221-E-133 -001. One of the authors, J.-H. Lin, would like to thank 95-2811-M-009-002 for providing Postdoctor fellowship.

References

[1] J.C. Knight, J. Arriaga, T.A. Birks, A. Ortigosa-Blanch, W.J. Wadsworth, and P.St.J. Russell, IEEE Photon. Technol. Lett. **12**, 807–809 (2000).
[2] P.St.J. Russell, Science **299**, 358–362 (2003).
[3] A.B. Fedotov, E.E. Serebryannikov, A.A. Ivanov, L.A. Mel'nikov, A.V. Shcherbakov, D.A. Sidorov-Biryukov, Ch.-K. Sun, M.V. Alfimov, and A.M. Zheltikov, Laser Phys. Lett. **3**, 301–305 (2006).
[4] S.O. Konorov, D.A. Akimov, A.A. Ivanov, M.V. Alfimov, A.B. Fedotov, D.A. Sidorov-Biryukov, L.A. Mel'nikov, A.V. Shcherbakov, I. Bugar, D. Chorvat, Jr., F. Uherek, D. Chorvat, and A.M. Zheltikov, Laser Phys. Lett. **1**, 402–405 (2004).
[5] J.K. Ranka, R.S. Windeler, and A.J. Stentz, Opt. Lett. **2**, 25–27 (2000).
[6] G. Genty, M. Lehtonen, H. Ludvigsen, J. Broeng, and M. Kaivola, Opt. Express. **10**, 1083–1098 (2002).
[7] W.H. Reeves, D.V. Skryabin, F. Biancalana, J.C. Knight, P.St.J. Russell, F. Ominetto, A. Efimov, and A.J. Taylor, Nature **424**, 511–515 (2003).
[8] I. Cristiani, R. Tediosi, L. Tartara, and V. Degiorgio, Opt. Express **12**, 124–135 (2004).
[9] J.H. Lin, C.C. Hsu, W.F. Hsieh, and K.H. Lin, Opt. Commun. **265**, 659–663 (2006).
[10] M. Lie Hu, C.Y. Wang, L. Chai, Y. Li, K.V. Dukel'skii, A.V. Khokhlov, V.S. Shevandin, Yu.N. Kondrat'ev, and A.M. Zheltikov, Laser Phys. Lett. **1**, 299–302 (2004).
[11] S.O. Konorov, D.A. Akimov, E.E. Serebryannikov, A.A. Ivanov, M.V. Alfimov, K.V. Dukel'skii, A.V. Khokhlov, V.S. Shevandin, Yu.N. Kondrat'ev, and A.M. Zheltikov, Laser Phys. Lett.**2**, 258–261 (2005).
[12] S.O. Konorov, E.E. Serebryannikov, P. Zhou, A.V. Khokhlov, V.S. Shevandin, K.V. Dukel'skii, Yu.N. Kondrat'ev, D.A. Sidorov-Biryukov, A.B. Fedotov, A.P. Tarasevitch, D. von der Linde, and A.M. Zheltikov, Laser Phys. Lett. **1**, 199–204 (2004).
[13] M.L. Hu, C.Y. Wang, E.E. Serebryannikov, Y.J. Song, Y.F. Li, L. Chai, K.V. Dukel'skii, A.V. Khokhlov, V.S. Shevandin, Yu.N. Kondrat'ev, and A. M. Zheltikov, Laser Phys. Lett. **2**, 306–309 (2006).
[14] M. Seefeldt, A. Heuer, and R. Menzel, Opt. Commun. **216**, 199–202 (2003).
[15] S. Coen, A.H.L. Chau, R. Leonhardt, J.D. Harvey, J.C. Knight, W.J. Wadsworth, and P.St.J. Russell, Opt. Lett. **26**, 1356–1358 (2001).
[16] S. Coen, A.H.L. Chau, R. Leonhardt, J.D. Harvey, J.C. Knight, W.J. Wadsworth, and P.St.J. Russell, J. Opt. Soc. Am. B. **19**, 753–764 (2002).
[17] W.J. Wadsworth, N. Joly, J.C. Knight, T.A. Birks, F. Biancalana, P.St.J. Russell, Opt. Express **12**, 299–399 (2004).
[18] V. Tombelaine, C. Lesvigne, P. Leproux, L. Grossard, V. Couderc, J.-L. Auguste, J.-M. Blondy, G. Huss, P.-H. Pioger, Opt. Express **13**, 7399–7404 (2005).
[19] S. Zhang, E. Wu, H. Pan, and H. Zeng, IEEE J. Quantum. Electron. **40**, 505–508 (2004).
[20] J.H. Lin, W.H. Yang, W.F. Hsieh, and K.H. Lin, Opt. Express **13**, 6323–6329 (2005).
[21] C. Honninger, R. Paschotta, F. Morier-Genoud, M. Moser, and U. Keller, J. Opt. Soc. Am. B **16**, 46–56 (1999).
[22] G.P. Agrawal, Nonlinear Fiber Optics (Academic Press, New York, 2001).